Cell Reports

Report

Mitochondrial Aging Defects Emerge in Directly Reprogrammed Human Neurons due to Their Metabolic Profile

Graphical Abstract

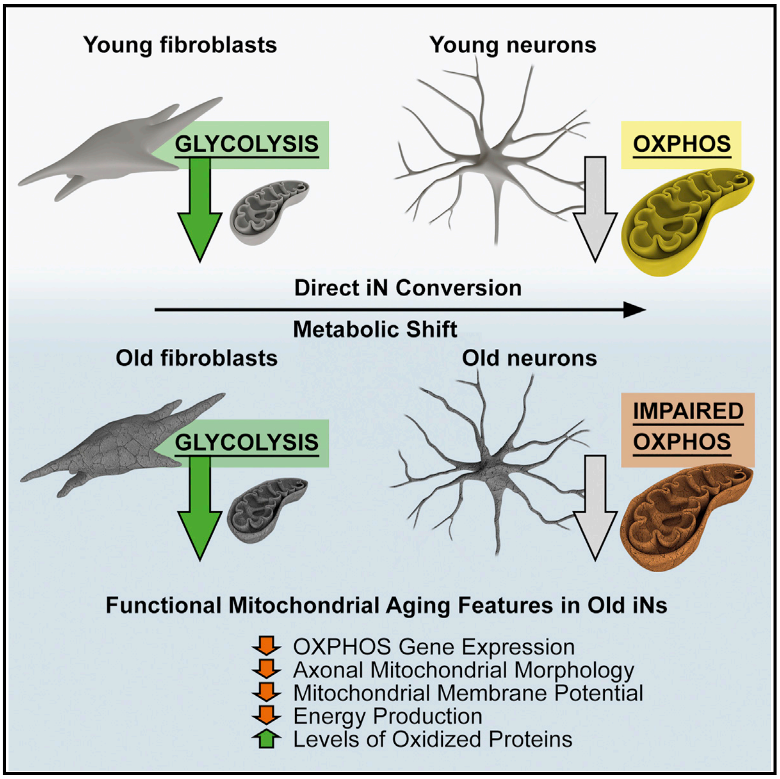

Authors

Yongsung Kim, Xinde Zheng, Zoya Ansari, ..., Tony Hunter, Jerome Mertens, Fred H. Gage

Correspondence

jmertens@salk.edu (J.M.), gage@salk.edu (F.H.G.)

In Brief

Kim et al. compared mitochondrial features in aging human fibroblasts and directly induced neurons (iNs). They find that only iNs display severe signs of mitochondrial aging defects and show that the metabolic shift during fibroblast-to-neuron conversion renders iNs particularly vulnerable to mitochondrial aging.

Highlights

- iNs from old human donor fibroblasts show reduced OXPHOS-related gene expression
- Old iNs display a variety of mitochondrial aging phenotypes
- Fibroblast-to-iN conversion is accompanied by a metabolic switch toward OXPHOS
- Neuronal bioenergetic profile causes increased vulnerability to mitochondrial aging

Data and Software Availability

E-MTAB-3037

Kim et al., 2018, Cell Reports *23*, 2550–2558
May 29, 2018
https://doi.org/10.1016/j.celrep.2018.04.105

OPEN ACCESS
CellPress

Cell Reports
Report

Mitochondrial Aging Defects Emerge in Directly Reprogrammed Human Neurons due to Their Metabolic Profile

Yongsung Kim,[1] Xinde Zheng,[2] Zoya Ansari,[1] Mark C. Bunnell,[1] Joseph R. Herdy,[1] Larissa Traxler,[1,3] Hyungjun Lee,[1] Apua C.M. Paquola,[1,4] Chrysanthi Blithikioti,[1] Manching Ku,[5,6] Johannes C.M. Schlachetzki,[7,8] Jürgen Winkler,[7] Frank Edenhofer,[3] Christopher K. Glass,[8] Andres A. Paucar,[1] Baptiste N. Jaeger,[1] Son Pham,[1] Leah Boyer,[1] Benjamin C. Campbell,[1] Tony Hunter,[2] Jerome Mertens,[1,3,*] and Fred H. Gage[1,9,*]

[1]Laboratory of Genetics, The Salk Institute for Biological Studies, 10010 North Torrey Pines Road, La Jolla, CA 92037, USA
[2]Molecular and Cell Biology Laboratory, The Salk Institute for Biological Studies, 10010 North Torrey Pines Road, La Jolla, CA 92037, USA
[3]Institute of Molecular Biology, Leopold-Franzens-University Innsbruck, Technikerstraβe 25, 6020 Innsbruck, Austria
[4]Lieber Institute for Brain Development, 855 North Wolfe Street, Suite 300, Baltimore, MD 21205, USA
[5]Next Generation Sequencing Core, The Salk Institute for Biological Studies, 10010 North Torrey Pines Road, La Jolla, CA 92037, USA
[6]Clinic for Pediatric Hematology and Oncology, Center for Pediatrics and Adolescent Medicine, University of Freiburg Medical Center, Mathildenstraβe 1, 79106 Freiburg im Breisgau, Germany
[7]Department of Molecular Neurology, Friedrich-Alexander University Erlangen-Nürnberg, 91054 Erlangen, Germany
[8]Department of Cellular and Molecular Medicine, University of California, San Diego, 9500 Gilman Drive, La Jolla, CA 92093-0651, USA
[9]Lead Contact
*Correspondence: jmertens@salk.edu (J.M.), gage@salk.edu (F.H.G.)
https://doi.org/10.1016/j.celrep.2018.04.105

SUMMARY

Mitochondria are a major target for aging and are instrumental in the age-dependent deterioration of the human brain, but studying mitochondria in aging human neurons has been challenging. Direct fibroblast-to-induced neuron (iN) conversion yields functional neurons that retain important signs of aging, in contrast to iPSC differentiation. Here, we analyzed mitochondrial features in iNs from individuals of different ages. iNs from old donors display decreased oxidative phosphorylation (OXPHOS)-related gene expression, impaired axonal mitochondrial morphologies, lower mitochondrial membrane potentials, reduced energy production, and increased oxidized proteins levels. In contrast, the fibroblasts from which iNs were generated show only mild age-dependent changes, consistent with a metabolic shift from glycolysis-dependent fibroblasts to OXPHOS-dependent iNs. Indeed, OXPHOS-induced old fibroblasts show increased mitochondrial aging features similar to iNs. Our data indicate that iNs are a valuable tool for studying mitochondrial aging and support a bioenergetic explanation for the high susceptibility of the brain to aging.

INTRODUCTION

Mitochondria are major generators of energy in our cells, and their age-related dysfunction is linked to impaired ATP production and an increase in oxidative damage (Bratic and Larsson, 2013). Dysfunctional mitochondria are major drivers of cellular aging and age-related disorders. Aging-related accumulation of macromolecular damage, including but not limited to mitochondrial DNA mutations, leads to increased proportions of impaired mitochondria within aged cells and tissues (Kujoth et al., 2005). Mitochondrial dysfunction is characterized by the loss of the mitochondrial membrane potential (MMP), which is directly linked to a loss of energy generated through the electron transport chain (ETC) that performs oxidative phosphorylation (OXPHOS); the failure of OXPHOS is believed to set the stage for the development of age-related disorders (Pickrell et al., 2011). Interestingly, inherited mitochondrial diseases that can be caused by mutations in genes encoded on the nuclear DNA, which encodes the vast majority of mitochondrial genes, or in genes that are encoded in mtDNA are often associated with neurodegenerative phenotypes, indicating a particular vulnerability of brain neurons to mitochondrial defects (Simon and Johns, 1999). Similarly, the human brain is an organ that is strongly affected by aging, and advanced age is by far the strongest risk factor for most neurodegenerative disorders (Wyss-Coray, 2016).

The generation of human neurons through induced pluripotent stem cell (iPSC) reprogramming and differentiation has been used to model mitochondrial disease-related phenotypes caused by mutations in nuclear genes (Chung et al., 2016). Modeling phenotypes caused by mtDNA mutations is more challenging, as the severity of mtDNA-based diseases is typically defined by the ratio of mtDNAs that carry the mutation within a mitochondrion, a phenomenon known as heteroplasmy (Stewart and Chinnery, 2015). Similarly, the increase of mtDNA mutations with aging can be recapitulated by investigating several heteroplasmic iPSC lines (Kang et al., 2016). However, progressive aging affects not only mtDNA but also other organelle structures, nuclear transcriptomics, and several cellular pathways that regulate mitochondria. Furthermore, as iPSC reprogramming erases cellular aging signatures (Miller et al., 2013), including mitochondrial phenotypes and nuclear transcriptomes (Prigione et al., 2011; Suhr et al., 2010), the usefulness of iPSCs for studying age-related phenomena that lie beyond DNA mutations is limited. Therefore, to investigate and link the specific susceptibility of neurons to aging and mitochondrial dysfunction, a human neuronal model that integrates known and as-yet-unknown mitochondrial aging phenotypes would be desirable. Directly converted induced neurons (iNs) from old human donor-derived fibroblasts possess important features of cellular aging, including global transcriptomic changes, nuclear pore defects, and DNA methylation, rendering them a valuable tool for the study of age-related neurodegenerative diseases (Huh et al., 2016; Mertens et al., 2015; Tang et al., 2017). Here, we specifically assessed endogenous human age-dependent mitochondrial aging phenotypes in iNs using our previously established iN system (Mertens et al., 2015).

RESULTS

Old Fibroblast-Derived iNs Show Decreased OXPHOS-Related Gene Expression

We have previously described the generation and purification of functional iNs from a cohort of aging human donors ranging in age from 0 to 89 years. Following at least 3 weeks of conversion, iN cultures consisted of a major fraction of excitatory neurons and a minor fraction of inhibitory neurons (Figures S1A–S1C; Mertens et al., 2015). Throughout this study, and similar to previous studies, we defined "young" cells as those derived from human donors younger than 40 years and "old" cells as those derived from donors aged 40 years and older (Figure 1A; Mertens et al., 2015). Here, we focused on 1,118 expressed mitochondrial genes selected based on the Human MitoCarta 2.0 project (human genes selected for high confidence of mitochondrial localization based on integrated proteomics, computation, and microscopy [Calvo et al., 2016]). We found that 70% of all mitochondrial genes were downregulated in old iNs compared to young iNs (Figure 1B). Interestingly, categorization of the mitochondrial genes into functional groups revealed that 93% of the genes that composed the mitochondrial ETC complexes I–V were downregulated in old iNs (Figure 1C). Also, genes that related to the tricarboxylic acid (TCA) cycle and the pentose phosphate pathway (PPP) were downregulated in old iNs, whereas genes that related to mitochondrial biogenesis or the pyruvate dehydrogenase complex (PDC) were not affected (Figure 1C). Among the ETC genes, complex I, V, III, and IV genes were all significantly affected (in that order by significance) (Figure 1D). Western blot analysis for SDHB (complex II [cII]), UQCRC2 (cIII), COXII (cIV, mtDNA-encoded), and ATP5A (cV) confirmed decreased protein levels of these representative ETC complex factors (Figures 1E and S1D). Furthermore, translation and transcription of the mtDNA plus-strand-encoded MT-ND1 were found to be decreased by qPCR and western blot, and expression of mitochondrial ribosomal proteins (MRPs) was also significantly decreased in old iNs (Figures S1E–S1G). These data indicate that aging alters mitochondrial OXPHOS-related gene expression and protein abundance in neurons.

iNs from Old Donors Show Impaired Mitochondrial Function

We next asked whether the observed transcriptional changes corresponded to functional impairment of mitochondria in old iNs. Axonal localization of mitochondria is vital to their function, and reduced axonal densities and the appearance of fragmented mitochondria are associated with impaired mitochondria in neurons (Chan, 2012; Sun et al., 2013). Using a lentiviral MitoEGFP reporter to label mitochondria, we detected significantly reduced mitochondrial densities in SMI-312-positive axons (Figures 2A, 2B, S2A, and S2B). Furthermore, we observed higher levels of mitochondrial fragmentation, as indicated by reduced mitochondrial length, as well as reduced mitochondrial coverage in the axons of old iNs (Figures 2B, S2A, and S2B). These morphological features are indicative of general mitochondrial dysfunction in old iNs, so we decided to next test the mitochondrial MMP, which is known to determine many mitochondrial functions (Chan, 2012; Mitchell, 1961; Saxton and Hollenbeck, 2012). To measure MMPs specifically in iN cells, we used fluorescence-activated cell sorting (FACS) analysis of human synapsin-1 promoter-driven blue fluorescent protein (hSyn::BFP)-labeled iNs with the green fluorescent cationic dye JC-1, which accumulates in red fluorescent aggregates in mitochondria with high MMPs (Figure 2C) (Smiley et al., 1991). We first gated for the BFP-positive neuronal population (Figure 2D) and then measured green and red JC-1 fluorescence in this population (Figure 2E). Young iNs showed significantly higher MMPs than old iNs, which showed an average 43% drop (Figure 2F). Next, to test whether this age-dependent loss of MMP was consequential for the total neuronal energy levels in young and old iNs, we purified iNs by polysialylated-neural cell adhesion molecule (PSA-NCAM) FACS and then measured ATP level in FACS-purified iNs. In line with the gene expression and morphological and MMP defects, we detected significantly lower total ATP levels in old neurons (Figure 2G). Oxyblot analysis revealed significantly increased levels of oxidized protein damage in old iN cultures, further indicating mitochondrial defects (Figures 2H and S2C). Furthermore, to test to what extent neuronal features downstream of mitochondria became impaired in old iNs, we assessed neurite beading and found that almost 50% of all neurites in old iN cultures showed axonal varicosities at 6 weeks in culture (Figures S2D and S2E). Consistently, and as early as 3 weeks in culture, synaptic transmission gene expression (GO: 0007270) was significantly decreased in old iNs (Figure S2F). While global antioxidant gene expression profiles of fibroblasts and iNs showed cell-type-specific differences, the major antioxidant genes *NURR1* (*NR4A2*) and *NRF2* (*NFE2L2*) did not show obvious expression differences between the cell types (Figures S2G–S2J). Interestingly, we found FOXO transcription factor transcripts to be slightly upregulated and FOXO3-repressed genes to be downregulated in old iNs (Figures S2K and S2L), whereas *HIF1A* and its target genes were not changed (Figures S2M and S2N). Together, these data show that directly converted iNs from young and old donor fibroblasts reflect broad functional defects associated with mitochondrial aging and provide a model to study bioenergetic aspects of human neuronal aging *in vitro*.

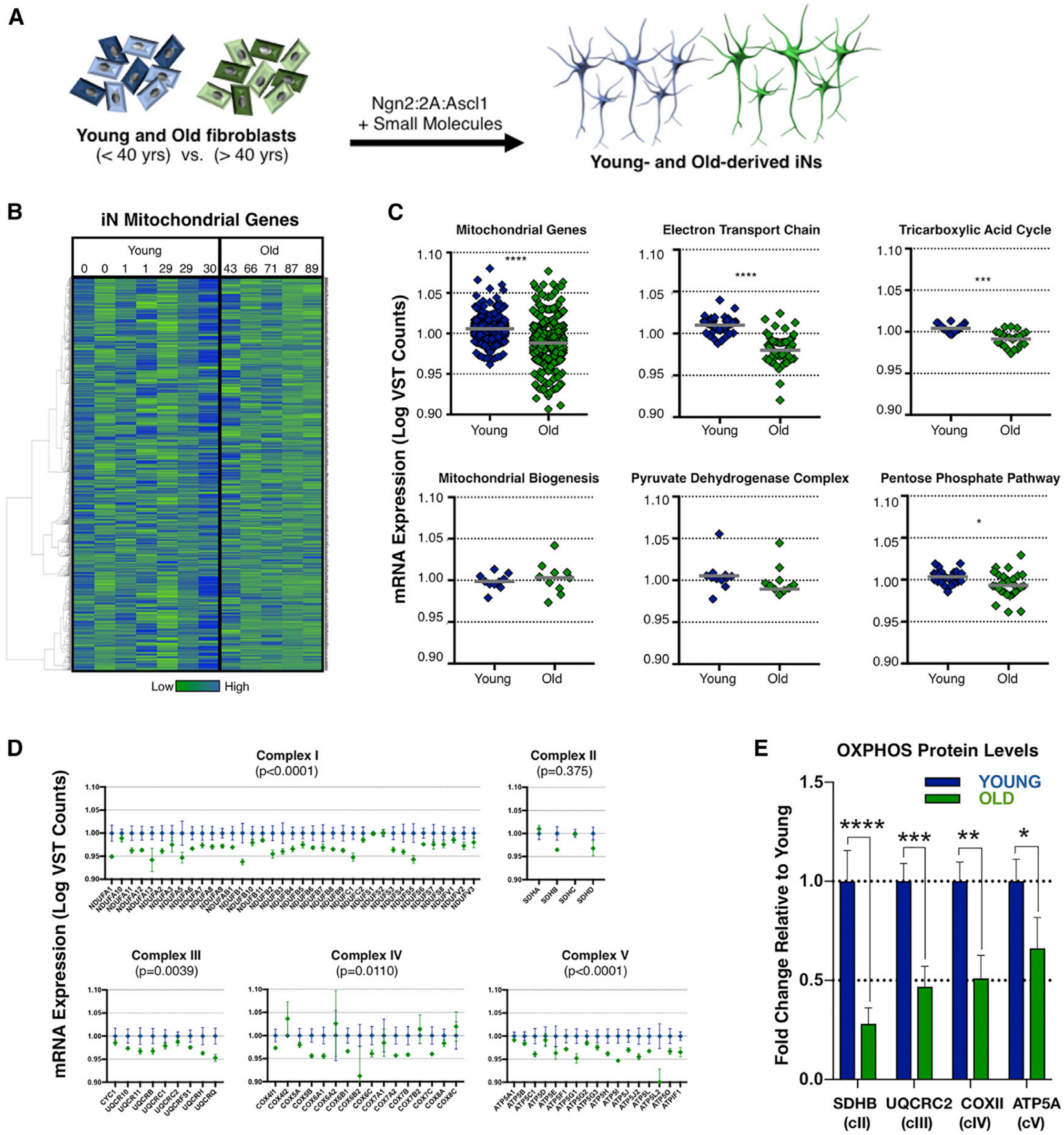

Figure 1. Age-Dependent Expression of Mitochondrial Genes in iNs

(A) Direct iN conversion of young and old fibroblasts using Ngn2-2A-Ascl1 and small-molecule enhancers.

(B) Heatmap of 1,118 mitochondrial genes in young (<40 years) and old (>40 years) purified iNs (n = 12 individuals, one RNA-seq profile each; see also Table S1 for donor information and Table S3).

(C) Expression of functional gene groups in young and old iNs. Logarithmic variance stabilizing transformation (VST) normalized counts; bars indicate mean values; dots represent genes; significance values were calculated by the non-parametric Wilcoxon test.

(D) Relative expression of ETC complex I, II, III, IV, and V in young and old iNs. VST normalized counts normalized to young; dots indicate mean ± SEM; significance was calculated by Wilcoxon test.

(E) Protein levels of indicated OXPHOS proteins in young and old iNs assessed by quantitative MitoProfile western blot (n = 6 individuals, 2 replicates). Significance values were calculated by t test. Representative blot in Figure S1D.

Significance values in this figure: *p < 0.05, **p < 0.01, ***p < 0.005, and ****p < 0.001.

iPSC-Derived Neurons from Aging Donors Show No Age-Related Mitochondrial Defects

Several groups have previously shown that iPSC reprogramming results in clonal cell lines with rejuvenated mitochondria (Lapasset et al., 2011; Prigione et al., 2011; Suhr et al., 2010) and that iPSC-derived neurons lack age-related phenotypes in general (Huh et al., 2016; Mertens et al., 2015; Miller et al., 2013; Tang et al., 2017). To confirm these observations with regard to our readouts and our present cohort, we analyzed iPSC-derived neurons from three of our donors (29, 43, and 71 years of age;

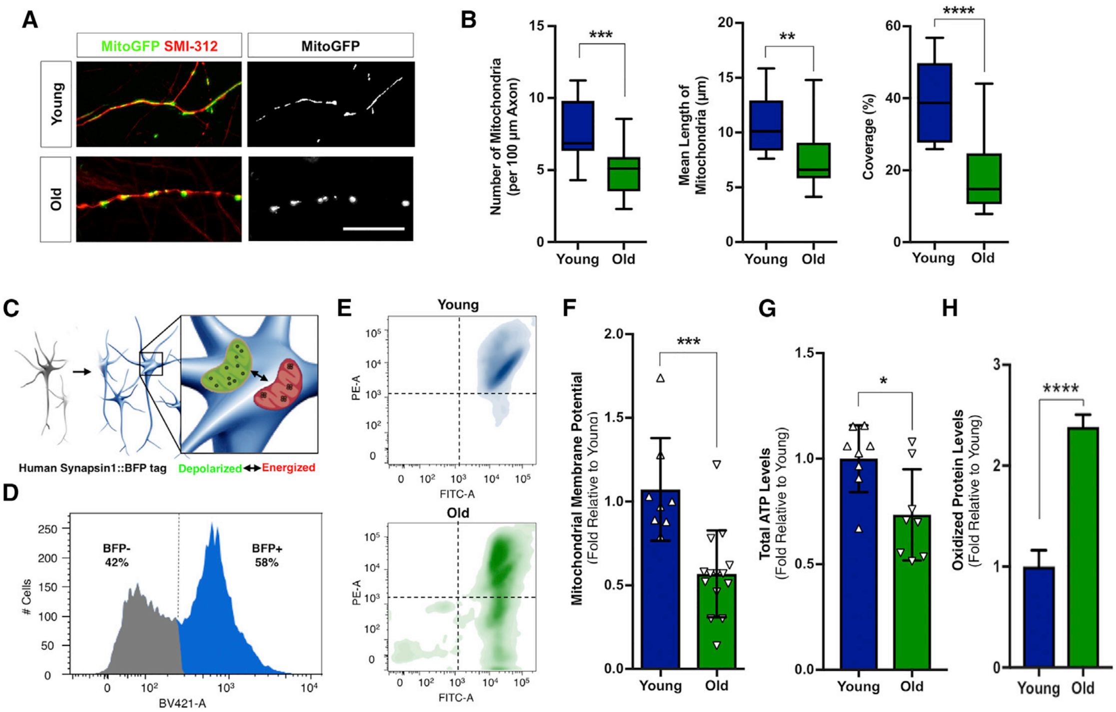

Figure 2. Mitochondrial Dysfunction in Young and Old iNs

(A) Representative fluorescence images of mitochondria (hSyn::MitoEGFP) in SMI-312-positive axons in young (1 year) and old (71 years) donor-derived iNs (see also Figures S2A and S2B). Scale bar, 20 µm.

(B) Quantification of axonal mitochondrial morphologies for densities, mean lengths, and coverage in young and old iNs (n = 7 individuals, 6 replicates each). Boxplots show 25th to 75th percentiles, bars indicate medians, and whiskers show ranges. Significance values were calculated by unpaired t tests (see also Figures S2A and S2B).

(C and D) hSyn::BFP-tagged iNs were gated (D) and analyzed for MMPs using the JC-1 dye (C).

(E) Representative JC-1 FACS density plots showing energized mitochondria in young iNs (1 year) and a loss of MMP in old iNs (71 years).

(F) Quantification of the MMP in young and old hSyn::BFP-positive iNs (n = 7 individuals, 3 replicates). Bar graph shows means ± SD, and triangles indicate individual measurements. Significance values were calculated by Mann-Whitney test.

(G) ATP levels in young and old purified iNs (6 individuals, 3 replicates). Bar graph shows means ± SD, and triangles indicate individual measurements. Significance values were calculated by Mann-Whitney test.

(H) Quantification of oxidized proteins as assessed by quantitative western blot (OxyBlot; 6 individuals, 2 replicates, representative blot in Figure S2C).

Significance values in this figure: *$p < 0.05$, **$p < 0.01$, ***$p < 0.005$, and ****$p < 0.001$.

Figure S3A), and consistent with previous data, we observed no age-dependent transcriptional differences in mitochondrial or OXPHOS gene expression as determined by RNA sequencing (RNA-seq) (Figure S3B). Furthermore, OXPHOS protein levels, mitochondrial morphologies in neurites, MMPs, total ATP levels, and levels of oxidized proteins were not different between the 29-, 43-, and 71-year-old iPSC-derived neurons (Figures S3C–S3J). These data confirm the previously described mitochondrial rejuvenation that follows iPSC differentiation and neuronal differentiation.

Old Primary Human Fibroblasts Show Only Mild Mitochondrial Aging Defects

Although both aging- and mutation-caused mitochondrial dysfunctions can cause multi-systemic dysfunctions, the brain is one of the organs most vulnerable to both aging and inherited mitochondria-associated diseases. To test this phenomenon in our model system, we asked to what extent the parental fibroblast cultures from which the iNs were derived possessed similar age-dependent mitochondrial impairments. To our surprise, RNA-seq analysis of the 12 young and old fibroblast cultures showed only a slight decrease in the Human MitoCarta 2.0 mitochondrial genes (Figure 3A). Overall, mitochondrial gene mRNA levels decreased 2.3 times less between young and old fibroblasts than they did between young and old iNs (Figure 3B). Similarly, while an age-related decrease of ETC genes was detectable in fibroblasts, the loss was also 2.3 times less pronounced than in the iN system, and other gene categories did not show significant age-related changes (Figures 3B and S4A). No loss of the ETC proteins SDHB, UQCRC2, COXII, and ATP5A could be detected in old fibroblasts (Figures 3C and S4B). Next, we performed a morphological analysis of MTC02 antibody-labeled mitochondria in fibroblasts (Figures 3D, S4C, and S4D), which also revealed no significant age-dependent differences in mitochondrial aspect ratios or form factors (Figures 3E, S4C, and S4D). MMP analysis detected a slight but significant 15% drop in MMP in old fibroblasts compared to young fibroblasts that, consistent with the

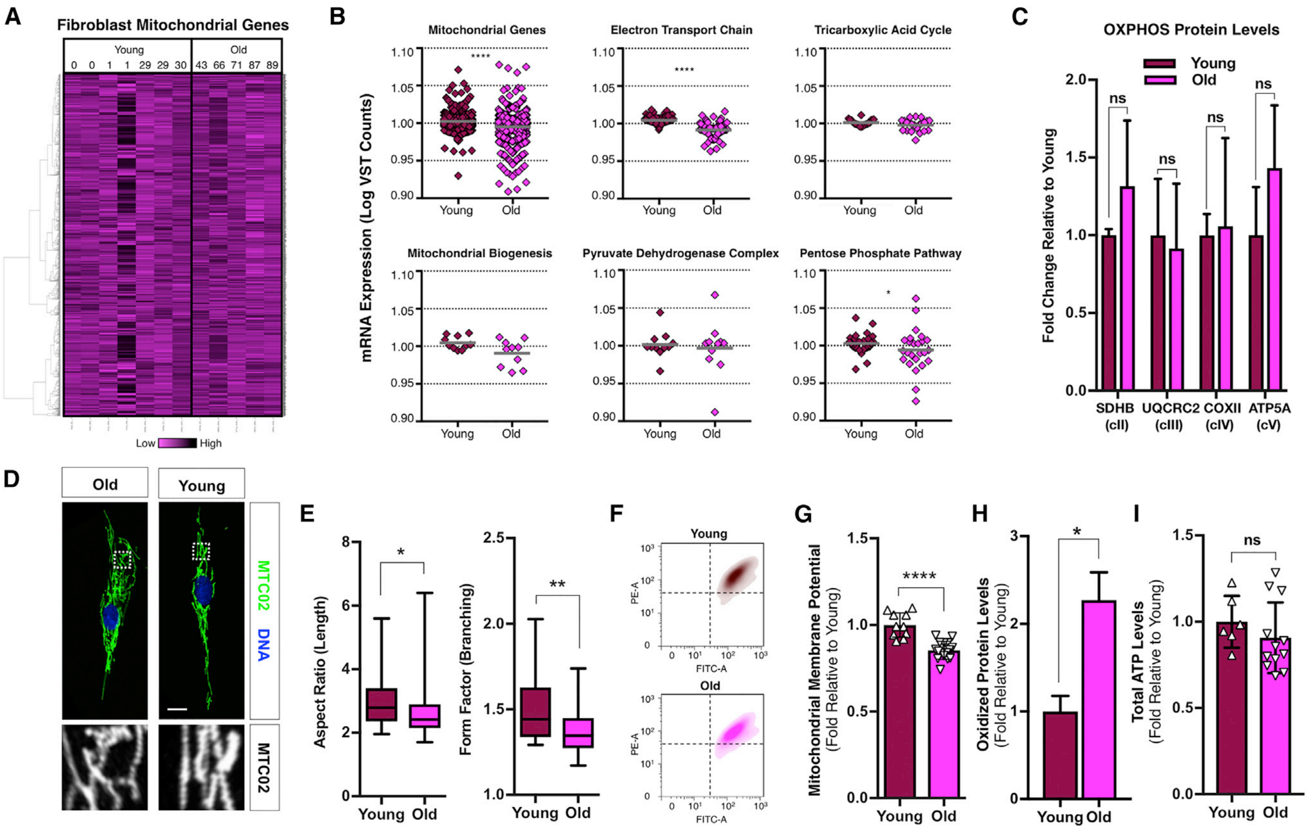

Figure 3. Mild Aging Phenotypes in Young and Old Fibroblasts

(A) Heatmap of mitochondrial genes in young (<40 years) and old (>40 years) primary human fibroblasts (n = 12 individuals, one RNA-seq profile each; see also Table S3).

(B) Expression of functional gene groups in young and old fibroblasts. Significance values were calculated by the non-parametric Wilcoxon test (see also Figure S4A for individual ETC genes).

(C) Protein levels of OXPHOS proteins in young and old fibroblasts assessed by quantitative western blot (n = 7 individuals, 3 replicates). Significance values were calculated by t test. Representative blot in Figure S4B.

(D) Representative fluorescence images of mitochondria (MTC02) in young (1 year) and old (71 years) fibroblasts (see also Figure S4D). Scale bar, 20 μm.

(E) Quantification of mitochondrial morphologies for aspect ratio (length) and form factor (branching) in fibroblasts (n = 7 individuals, 10 replicates). Boxplots show 25th to 75th percentiles; bars indicate medians, and whiskers show ranges. Significance values were calculated by unpaired t tests (see also Figures S4C and S4D).

(F) Representative MMP (JC-1) FACS density plots of young (0 year) and old (89 years) fibroblasts.

(G) Quantification in young and old fibroblasts (n = 7 individuals, 3 replicates). Bar graph shows means ± SD, and triangles indicate individual measurements. Significance values were calculated by Mann-Whitney test.

(H) Quantification of oxidized proteins as assessed by quantitative western blot (OxyBlot; 6 individuals, a representative blot in Figure S4E).

(I) Total ATP levels in young and old fibroblasts (6 individuals, 3 replicates). Bar graph shows means ± SD; triangles indicate individual measurements. Significance values were calculated by Mann-Whitney test.

ns, not significant. Significance values in this figure: *$p < 0.05$, **$p < 0.01$, and ****$p < 0.001$.

transcriptome data, was 2.9 times weaker than the aging effect measured in iNs from the same donors (Figures 3F and 3G). Furthermore, while we detected higher levels of oxidized proteins in old fibroblasts than in young ones (Figures 3H and S4E), measurements of total ATP levels detected no decrease in old fibroblasts (Figure 3I). Together, these data show that, although old fibroblast-derived iNs showed severe mitochondrial defects, their parental fibroblasts showed only mild age-related phenotypes. We therefore reasoned that our model system might recapitulate aspects of the neuronal specificity of age-dependent mitochondrial dysfunction and might be useful to further explore this phenomenon.

A Metabolic Shift between Fibroblasts and Neurons toward OXPHOS Underlies the Neuron-Specific Vulnerability of Mitochondria to Aging

Given that mitochondria showed strong age-dependent defects in human iNs whereas the same old mitochondria appeared largely undisturbed in fibroblasts, we asked whether general bioenergetic differences between the two cell types might explain this observation. Comparing the expression of metabolic genes in fibroblasts and iNs, we found that ETC cI–V genes as well as TCA cycle, PDC, and mitochondrial biogenesis genes were expressed at higher levels in iNs than in fibroblasts, indicating much higher levels of mitochondrial OXPHOS in iNs

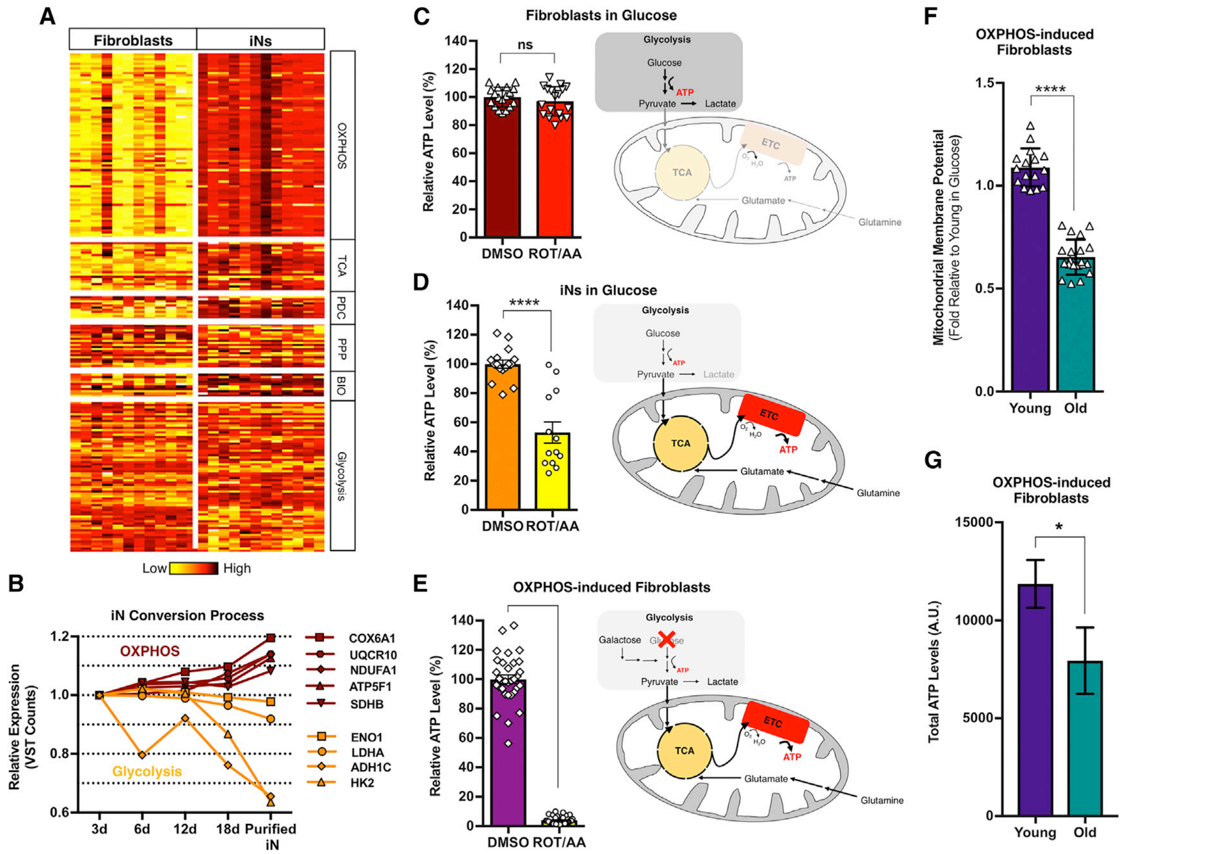

Figure 4. Metabolic Switch to OXPHOS Induces Mitochondrial Aging Phenotypes

(A) Heatmap of metabolic genes in human primary fibroblasts and FACS-purified iNs (n = 12 individuals, one iN and one fibroblast RNA-seq each; see also Table S3).

(B) Expression of five representative OXPHOS genes and four canonical glycolysis genes over time during fibroblast-to-iN conversion (four time points and purified iNs from day 18). VST normalized counts were normalized to day 3.

(C–E) Relative ATP levels and schematic drawing of metabolic pathways active in fibroblasts (C), purified iNs (D), and OXPHOS-induced fibroblasts (E) treated with ROT/AA or vehicle for 6 hr (n = 8 individuals per cell type; 4 replicates). Bars represent means ± SD; symbols mark individual measurements. Significance values were calculated by t test.

(F) MMP (JC-1) in young and old OXPHOS-induced fibroblasts (n = 7 individuals; 4 replicates). Bars represent means ± SD. Symbols mark individual measurements. Significance values were calculated by t test.

(G) Total ATP levels in young and old OXPHOS-induced fibroblasts (n = 8 individuals; 4 replicates). Bars represent means ± SD. Symbols mark individual measurements. Significance values were calculated by t test.

Significance values in this figure: *p < 0.05 and ****p < 0.001.

(Figures 4A and S2). Mitochondrial ribosomal genes are also expressed at higher levels in iNs, indicating a higher activity of the mitochondrial transcription and translational machinery (Figure S4F). In contrast, PPP and glycolysis genes did not show a clear difference between fibroblasts and iNs (Figure 4A). We next tested the expression of five representative OXPHOS genes (*SDHB*, *ATP5F1*, *NDUFA1*, *UQCR10*, and *COX6A1*) over the time course of fibroblast-to-iN conversion (days 3, 6, 12, 18, and FACS-purified iNs), which revealed a progressive upregulation of OXPHOS/ETC gene expression during conversion (Figure 4B). Conversely, the key glycolysis genes *ENO1*, *LDHA*, *ADH1C*, and *HK2* became downregulated in the process, indicating a decrease in canonical glycolysis in neurons (Figure 4B). To test the extent to which ATP production in the two cell types depended on mitochondrial OXPHOS, we treated fibroblasts and FACS-purified iNs with rotenone and antimycin-A (ROT/AA) and measured total ATP levels after 6 hr. While ATP production in fibroblasts did not decrease significantly in response to ROT/AA (Figure 4C), iNs lost 47% of their ATP levels as a result of the treatment (Figure 4D). As iNs bioenergetically depend more on mitochondrial OXPHOS whereas fibroblasts derive their ATP predominantly by performing glycolysis, neuronal mitochondria likely display stronger aging phenotypes because of their increased work burden. We therefore asked whether old fibroblasts, when artificially forced to perform OXPHOS, would show mitochondrial aging phenotypes similar to neurons. To induce OXPHOS in fibroblasts, the cells were cultured in glucose-depleted but galactose-containing culture medium for 3 days. Under these conditions, ROT/AA treatment for 6 hr led to a near-complete loss of the fibroblasts' ATP, indicating a successful induction of OXPHOS and loss of glycolysis (Figure 4E). We next measured the MMP of old and young OXPHOS-induced fibroblasts and, indeed, similar to the iNs, old OXPHOS-induced fibroblasts showed 40% lower MMP levels than young OXPHOS-induced fibroblasts (Figure 4F). Consequentially, and similar to the observations in iNs, old OXPHOS-induced fibroblasts had 33% lower total ATP levels (Figure 4G). These data indicate that a cell type's susceptibility to mitochondrial aging critically depends on the level of OXPHOS it performs and that the metabolic profile of neurons might render them particularly vulnerable to mitochondrial aging.

Taken together, our results indicated that fibroblast-derived iNs showed broad signs of mitochondrial aging, making them valuable for the study of age-related bioenergetic dysfunctions directly in human neurons. The data further emphasize the importance of mitochondrial aging specifically for neuronal cells and point to a bioenergetic explanation for the type selectivity of mitochondria-associated cellular dysfunctions.

DISCUSSION

Aging is a degenerative process caused by the accumulation of macromolecular damage that leads to organelle, cell, and eventually tissue dysfunction. Neurons are postmitotic cells born during development and have very limited capacity for self-renewal in the brain over a person's life span. The age-dependent decline of neuronal mitochondrial function is one of the major hallmarks of the aging brain (Payne and Chinnery, 2015). In addition to age-dependent global transcriptome changes and defects in nucleocytoplasmic shuttling (Mertens et al., 2015), we show here that iNs directly reprogrammed from primary human skin fibroblasts derived from old donors displayed typical aspects of human neuronal mitochondrial aging.

Previous microarray-based transcriptome studies in both aging rats and aging human prefrontal cortex samples (Lu et al., 2004) have found that the expression of multiple, nuclear-encoded mitochondrial genes gradually declines during aging. Consistently, old iNs showed decreased expression of more than two-thirds of all expressed mitochondrial genes (Calvo et al., 2016) and a specific reduction in OXPHOS-related genes, which have been considered to impair respiratory function in the old brain (Manczak et al., 2005). Furthermore, similar to our observations in iNs, mitochondria in the young rhesus monkey brain have spheroid elongated tubular structures whereas old mitochondria often show altered shapes (Hara et al., 2014). Morphological changes and ATP production loss are typical signs of dysfunctional mitochondria and are, like most mitochondrial functions, controlled by the MMP (Ahmad et al., 2013; Miller and Sheetz, 2004). Thus, the reduced MMPs in old iNs represent a major hallmark of bona fide mitochondrial aging in our model system. Taken together, our results show that old human donor fibroblast-derived iNs display a broad range of aging signatures that have been previously described in human post-mortem human brain samples. iN technology thus represents a valuable tool to study functional phenotypes of mitochondrial aging in human neurons.

The human brain consumes up to 20% of the energy used by the entire human body, more than any other single organ. Mitochondrial OXPHOS provides this massive amount of ATP for the neurons, and the disease- or age-dependent failures of mitochondria due to mutations or toxins typically primarily affect the brain more than other organs (Hall et al., 2012). In our system of young and old fibroblasts and directly derived young and old iNs, we observed a similar neuron-specific vulnerability to mitochondrial aging. Consistent with our data, it has previously been shown that, during differentiation of iPSC-derived neural progenitors to postmitotic neurons as well as during iN conversion, cells undergo a metabolic shift from glycolysis to OXPHOS. This switch proved to be very important for the establishment of neuronal identity, as neuronal differentiation/conversion failed when the canonical glycolysis genes *LDHA* and *HK2* were overexpressed during differentiation (Zheng et al., 2016) or when OXPHOS was prevented by oligomycin A treatment (Gascón et al., 2016). Consistently, *LDHA* and *HK2* became downregulated during iN conversion, and prolonged treatments with ROT/AA were found to be very toxic to our iNs, further supporting the view that active OXPHOS is a necessity for human neuronal identity *in vitro*. During short-term ROT/AA exposure, however, iNs appeared to be competent in generating ATP through glycolysis and/or other pathways. This metabolic plasticity might be a useful mechanism for human neurons to compensate for temporary oxygen shortage (e.g., stroke) or mitochondrial failure (e.g., toxins). However, this plasticity might not be sufficient to compensate for age-related mitochondrial dysfunction over long periods of time, whereas optimizing oxygen supply for OXPHOS appears to be a successful strategy to mitigate age-dependent cognitive decline (Barnes, 2015). Furthermore, OXPHOS induction in fibroblasts for only 3 days was sufficient to reveal age-dependent mitochondrial defects in MMP and ATP generation similar to iNs. These data suggest that the bioenergetic profile of neurons is the primary reason for the specific vulnerability of the brain to age-dependent mitochondrial decline, and we support a model in which mitochondrial aging defects require a certain threshold of mitochondrial activity before unfolding. In addition, a temporary overshoot of oxidative stress that has been described to occur during iN conversion might further contribute to eliciting mitochondrial defects in already handicapped old iNs (Gascón et al., 2016).

We feel that iN technology is both unique and complementary to iPSC reprogramming paradigms in the study of mitochondrial aging. Unlike in iNs, each iPSC line is a clonal derivative of one single fibroblast. Due to the fact that iPSC reprogramming and expansion are highly selective processes, the generation of heteroplasmic iPSC lines from mtDNA disease patients allows comparison of "mutation-rich" to "mutation-free" iPSC lines from the same donor (Fujikura et al., 2012; Inak et al., 2017). While this is a clear advantage for iPSCs when it comes to the investigation of a certain mtDNA mutation, such model iPSC lines do not necessarily reflect the genetic state in a patient's cells (Folmes et al., 2013; Hatakeyama et al., 2015; Hämäläinen et al., 2013). In this current study, iNs have the advantage that they do not involve a clonal selection process and do not require cell division (Fishman et al., 2015; Mertens et al., 2016), so iN cultures can be expected to reflect the heteroplasmic state of the donor and most likely also contain other non-mtDNA-related drivers of mitochondrial aging that are lost during iPSC reprogramming and proliferation. This advantage, together with the general transcriptomic retention of age in iNs, renders iNs an interesting human model system to study neuronal phenotypes that involve biological aging, including mitochondrial decay.

EXPERIMENTAL PROCEDURES

Further details and an outline of resources used in this work can be found in Supplemental Experimental Procedures.

Direct Conversion of Human Fibroblasts into iNs

iN conversion of primary human dermal fibroblasts was previously described. Briefly, healthy donor-derived fibroblasts (0–89 years of age) were obtained from the Coriell Institute Cell Repository, the University Hospital in Erlangen, and ATCC (Table S1). Protocols were previously approved by the Salk Institute Institutional Review Board, and informed consent was obtained from all subjects. The fibroblasts were lentivirally transduced to express Ngn2:2A: Ascl1controlled by a tetOn system. Direct conversion was performed over 3–6 weeks before characterization (Table S2). A more detailed description of the method can be found in Supplemental Experimental Procedures.

MMP Analysis

MMP was assayed using the JC-1 lipophilic cationic dye (Life Technologies). hSyn::BFP-labeled iNs or fibroblasts were dissociated to single cells using TrypLE Express, washed twice, resuspended in 1 mL of warm 2 μM JC-1 diluted in the media and incubated at 37°C for 15–20 min. The cells were washed twice and resuspended in warm PBS, and then the green and red fluorescence of JC-1 dye was quantitated by flow cytometry (LSRII; Becton Dickinson). Histogram plots of green and red fluorescence were created to determine the red/green intensity ratio using FlowJo 10 software (Tree Star).

OXPHOS Induction in Fibroblasts

The fibroblasts were washed twice with PBS, then changed into galactose media (DMEM deprived of glucose; Invitrogen; 11966-025) supplemented with 5 mM galactose and 10% fetal bovine serum (FBS). The cells were incubated for 3 days until harvest.

Statistical Analysis

Statistical values for RNA-seq data were corrected for false-discovery rates (FDRs) using the Benjamini-Hochberg method implemented in R. Statistical tests of quantitative data were calculated using GraphPad Prism 7 software with the method indicated for each figure. Significance evaluation are marked as *$p < 0.05$, **$p < 0.01$, ***$p < 0.005$, and ****$p < 0.001$.

DATA AND SOFTWARE AVAILABILITY

The accession number for all raw RNA-seq data reported in this study is EMBL-EBI ArrayExpress: E-MTAB-3037.

SUPPLEMENTAL INFORMATION

Supplemental Information includes Supplemental Experimental Procedures, four figures, and three tables and can be found with this article online at https://doi.org/10.1016/j.celrep.2018.04.105.

ACKNOWLEDGMENTS

We thank the Coriell Institute for primary human fibroblast lines and Mary Lynn Gage for editorial comments. The study was supported by the Paul G. Allen Family Foundation, the National Institute on Aging (R01-AG056306-01 and K99-AG056679-01), the Austrian Science Fund FWF (SPIN doctoral school), Shiley-Marcos Alzheimer's Disease Research Center at the University of California, San Diego (UCSD), the JPB Foundation, the Glenn Foundation Center for Aging Research, the American Federation for Aging Research (AFAR), the Leona M. and Harry B. Helmsley Charitable Trust (2012-PG-MED002), Annette Merle-Smith, CIRM (TR2-01778), The G. Harold and Leila Y. Mathers Charitable Foundation, and the 2014 NARSAD Young Investigator Grant from the Brain & Behavior Research Foundation. The study was also supported by National Cancer Institute (CA014195, CA080100, and CA082683) to T.H., who is an American Cancer Society Professor and the Renato Dulbecco Chair in Cancer Research.

AUTHOR CONTRIBUTIONS

Conception, Design, and Writing of the Manuscript, Y.K., J.M., and F.H.G.; iN Conversions and Molecular Assays, Y.K., X.Z., Z.A., M.C.B., J.R.H., L.T., H.L., C.B., M.K., and J.M.; Bioinformatics Analysis, A.C.M.P. and J.M.; Generation, Differentiation, and Analysis of iPSCs, Y.K., C.B., J.C.M.S., C.K.G., A.A.P., B.N.J., S.P., L.B., and B.C.C.; Data Interpretation, Contribution to Experimental Design, and Editing of the Manuscript, Y.K., X.Z., Z.A., M.C.B., J.R.H., H.L., A.C.M.P., C.B., F.E., T.H., J.M., and F.H.G.; Derivation of Human Fibroblasts, J.C.M.S. and J.W.

DECLARATION OF INTERESTS

The authors declare no competing financial interests.

Received: August 4, 2017
Revised: January 19, 2018
Accepted: April 19, 2018
Published: May 29, 2018

REFERENCES

Ahmad, T., Aggarwal, K., Pattnaik, B., Mukherjee, S., Sethi, T., Tiwari, B.K., Kumar, M., Micheal, A., Mabalirajan, U., Ghosh, B., et al. (2013). Computational classification of mitochondrial shapes reflects stress and redox state. Cell Death Dis. *4*, e461.

Barnes, J.N. (2015). Exercise, cognitive function, and aging. Adv. Physiol. Educ. *39*, 55–62.

Bratic, A., and Larsson, N.-G. (2013). The role of mitochondria in aging. J. Clin. Invest. *123*, 951–957.

Calvo, S.E., Clauser, K.R., and Mootha, V.K. (2016). MitoCarta2.0: an updated inventory of mammalian mitochondrial proteins. Nucleic Acids Res. *44* (*D1*), D1251–D1257.

Chan, D.C. (2012). Fusion and fission: interlinked processes critical for mitochondrial health. Annu. Rev. Genet. *46*, 265–287.

Chung, S.Y., Kishinevsky, S., Mazzulli, J.R., Graziotto, J., Mrejeru, A., Mosharov, E.V., Puspita, L., Valiulahi, P., Sulzer, D., Milner, T.A., et al. (2016). Parkin and PINK1 patient iPSC-derived midbrain dopamine neurons exhibit mitochondrial dysfunction and α-synuclein accumulation. Stem Cell Reports *7*, 664–677.

Fishman, V.S., Shnayder, T.A., Orishchenko, K.E., Bader, M., Alenina, N., and Serov, O.L. (2015). Cell divisions are not essential for the direct conversion of fibroblasts into neuronal cells. Cell Cycle *14*, 1188–1196.

Folmes, C.D.L., Martinez-Fernandez, A., Perales-Clemente, E., Li, X., McDonald, A., Oglesbee, D., Hrstka, S.C., Perez-Terzic, C., Terzic, A., and Nelson, T.J. (2013). Disease-causing mitochondrial heteroplasmy segregated within induced pluripotent stem cell clones derived from a patient with MELAS. Stem Cells *31*, 1298–1308.

Fujikura, J., Nakao, K., Sone, M., Noguchi, M., Mori, E., Naito, M., Taura, D., Harada-Shiba, M., Kishimoto, I., Watanabe, A., et al. (2012). Induced pluripotent stem cells generated from diabetic patients with mitochondrial DNA A3243G mutation. Diabetologia *55*, 1689–1698.

Gascón, S., Murenu, E., Masserdotti, G., Ortega, F., Russo, G.L., Petrik, D., Deshpande, A., Heinrich, C., Karow, M., Robertson, S.P., et al. (2016). Identification and successful negotiation of a metabolic checkpoint in direct neuronal reprogramming. Cell Stem Cell *18*, 396–409.

Hall, C.N., Klein-Flügge, M.C., Howarth, C., and Attwell, D. (2012). Oxidative phosphorylation, not glycolysis, powers presynaptic and postsynaptic mechanisms underlying brain information processing. J. Neurosci. *32*, 8940–8951.

Hämäläinen, R.H., Manninen, T., Koivumäki, H., Kislin, M., Otonkoski, T., and Suomalainen, A. (2013). Tissue- and cell-type-specific manifestations of heteroplasmic mtDNA 3243A>G mutation in human induced pluripotent stem cell-derived disease model. Proc. Natl. Acad. Sci. USA *110*, E3622–E3630.

Hara, Y., Yuk, F., Puri, R., Janssen, W.G.M., Rapp, P.R., and Morrison, J.H. (2014). Presynaptic mitochondrial morphology in monkey prefrontal cortex correlates with working memory and is improved with estrogen treatment. Proc. Natl. Acad. Sci. USA *111*, 486–491.

Hatakeyama, H., Katayama, A., Komaki, H., Nishino, I., and Goto, Y. (2015). Molecular pathomechanisms and cell-type-specific disease phenotypes of MELAS caused by mutant mitochondrial tRNA(Trp). Acta Neuropathol. Commun. *3*, 52.

Huh, C.J., Zhang, B., Victor, M.B., Dahiya, S., Batista, L.F., Horvath, S., and Yoo, A.S. (2016). Maintenance of age in human neurons generated by microRNA-based neuronal conversion of fibroblasts. eLife *5*, e18648.

Inak, G., Lorenz, C., Lisowski, P., Zink, A., Mlody, B., and Prigione, A. (2017). Concise review: induced pluripotent stem cell-based drug discovery for mitochondrial disease. Stem Cells *35*, 1655–1662.

Kang, E., Wang, X., Tippner-Hedges, R., Ma, H., Folmes, C.D.L., Gutierrez, N.M., Lee, Y., Van Dyken, C., Ahmed, R., Li, Y., et al. (2016). Age-related accumulation of somatic mitochondrial DNA mutations in adult-derived human iPSCs. Cell Stem Cell *18*, 625–636.

Kujoth, G.C., Hiona, A., Pugh, T.D., Someya, S., Panzer, K., Wohlgemuth, S.E., Hofer, T., Seo, A.Y., Sullivan, R., Jobling, W.A., et al. (2005). Mitochondrial DNA mutations, oxidative stress, and apoptosis in mammalian aging. Science *309*, 481–484.

Lapasset, L., Milhavet, O., Prieur, A., Besnard, E., Babled, A., Aït-Hamou, N., Leschik, J., Pellestor, F., Ramirez, J.M., De Vos, J., et al. (2011). Rejuvenating senescent and centenarian human cells by reprogramming through the pluripotent state. Genes Dev. *25*, 2248–2253.

Lu, T., Pan, Y., Kao, S.-Y., Li, C., Kohane, I., Chan, J., and Yankner, B.A. (2004). Gene regulation and DNA damage in the ageing human brain. Nature *429*, 883–891.

Manczak, M., Jung, Y., Park, B.S., Partovi, D., and Reddy, P.H. (2005). Time-course of mitochondrial gene expressions in mice brains: implications for mitochondrial dysfunction, oxidative damage, and cytochrome c in aging. J. Neurochem. *92*, 494–504.

Mertens, J., Paquola, A.C.M., Ku, M., Hatch, E., Böhnke, L., Ladjevardi, S., McGrath, S., Campbell, B., Lee, H., Herdy, J.R., et al. (2015). Directly reprogrammed human neurons retain aging-associated transcriptomic signatures and reveal age-related nucleocytoplasmic defects. Cell Stem Cell *17*, 705–718.

Mertens, J., Marchetto, M.C., Bardy, C., and Gage, F.H. (2016). Evaluating cell reprogramming, differentiation and conversion technologies in neuroscience. Nat. Rev. Neurosci. *17*, 424–437.

Miller, K.E., and Sheetz, M.P. (2004). Axonal mitochondrial transport and potential are correlated. J. Cell Sci. *117*, 2791–2804.

Miller, J.D., Ganat, Y.M., Kishinevsky, S., Bowman, R.L., Liu, B., Tu, E.Y., Mandal, P.K., Vera, E., Shim, J.-W., Kriks, S., et al. (2013). Human iPSC-based modeling of late-onset disease via progerin-induced aging. Cell Stem Cell *13*, 691–705.

Mitchell, P. (1961). Coupling of phosphorylation to electron and hydrogen transfer by a chemi-osmotic type of mechanism. Nature *191*, 144–148.

Payne, B.A.I., and Chinnery, P.F. (2015). Mitochondrial dysfunction in aging: much progress but many unresolved questions. Biochim. Biophys. Acta *1847*, 1347–1353.

Pickrell, A.M., Fukui, H., Wang, X., Pinto, M., and Moraes, C.T. (2011). The striatum is highly susceptible to mitochondrial oxidative phosphorylation dysfunctions. J. Neurosci. *31*, 9895–9904.

Prigione, A., Hossini, A.M., Lichtner, B., Serin, A., Fauler, B., Megges, M., Lurz, R., Lehrach, H., Makrantonaki, E., Zouboulis, C.C., and Adjaye, J. (2011). Mitochondrial-associated cell death mechanisms are reset to an embryonic-like state in aged donor-derived iPS cells harboring chromosomal aberrations. PLoS One *6*, e27352.

Saxton, W.M., and Hollenbeck, P.J. (2012). The axonal transport of mitochondria. J. Cell Sci. *125*, 2095–2104.

Simon, D.K., and Johns, D.R. (1999). Mitochondrial disorders: clinical and genetic features. Annu. Rev. Med. *50*, 111–127.

Smiley, S.T., Reers, M., Mottola-Hartshorn, C., Lin, M., Chen, A., Smith, T.W., Steele, G.D., Jr., and Chen, L.B. (1991). Intracellular heterogeneity in mitochondrial membrane potentials revealed by a J-aggregate-forming lipophilic cation JC-1. Proc. Natl. Acad. Sci. USA *88*, 3671–3675.

Stewart, J.B., and Chinnery, P.F. (2015). The dynamics of mitochondrial DNA heteroplasmy: implications for human health and disease. Nat. Rev. Genet. *16*, 530–542.

Suhr, S.T., Chang, E.-A., Tjong, J., Alcasid, N., Perkins, G.A., Goissis, M.D., Ellisman, M.H., Perez, G.I., and Cibelli, J.B. (2010). Mitochondrial rejuvenation after induced pluripotency. PLoS One *5*, e14095–e14099.

Sun, T., Qiao, H., Pan, P.-Y., Chen, Y., and Sheng, Z.-H. (2013). Motile axonal mitochondria contribute to the variability of presynaptic strength. Cell Rep. *4*, 413–419.

Tang, Y., Liu, M.-L., Zang, T., and Zhang, C.-L. (2017). Direct reprogramming rather than iPSC-based reprogramming maintains aging hallmarks in human motor neurons. Front. Mol. Neurosci. *10*, 359.

Wyss-Coray, T. (2016). Ageing, neurodegeneration and brain rejuvenation. Nature *539*, 180–186.

Zheng, X., Boyer, L., Jin, M., Mertens, J., Kim, Y., Ma, L., Ma, L., Hamm, M., Gage, F.H., and Hunter, T. (2016). Metabolic reprogramming during neuronal differentiation from aerobic glycolysis to neuronal oxidative phosphorylation. eLife *5*, 859.

Cell Reports, Volume *23*

Supplemental Information

Mitochondrial Aging Defects Emerge in Directly Reprogrammed Human Neurons due to Their Metabolic Profile

Yongsung Kim, Xinde Zheng, Zoya Ansari, Mark C. Bunnell, Joseph R. Herdy, Larissa Traxler, Hyungjun Lee, Apua C.M. Paquola, Chrysanthi Blithikioti, Manching Ku, Johannes C.M. Schlachetzki, Jürgen Winkler, Frank Edenhofer, Christopher K. Glass, Andres A. Paucar, Baptiste N. Jaeger, Son Pham, Leah Boyer, Benjamin C. Campbell, Tony Hunter, Jerome Mertens, and Fred H. Gage

Figure S1. Neuronal subtype and mitochondrial characterization of aging iNs, Related to Figure 1

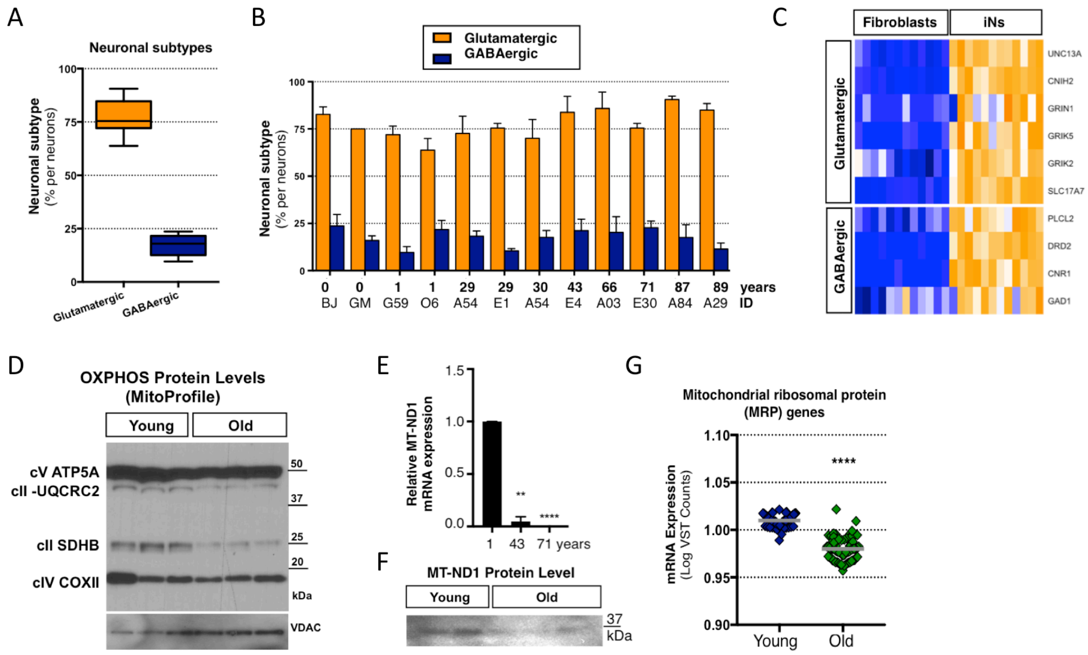

(**A**-**B**) Average fractions of glutamatergic (vGlut1/βIII-tubulin-positive) and GABAergic (GABA/Map2ab-positive) iNs across all 12 donors (**A**), and per donor (**B**).

(**C**) Heatmap showing relative expression of the glutamatergic neuron-specific genes Unc-13 homolog A (*UNC13A*), AMPA receptor auxiliary protein 2 (*CNIH2*), NMDA1 (*GRIN1*), GluK5 (*GRIK5*), GluK2 (*GRIK2*) and vGLUT1 (*SLC17A7*), and the GABAergic neuron-specific genes Phospholipase C like 2 (*PLCL2*), Dopamine Receptor D2 (*DRD2*), Cannabinoid receptor 1 (*CNR1*) and Glutamate decarboxylase 1 (*GAD1*). Blue = low expression, orange = high expression; normalized by row)

(**D**) Representative MitoProfile blot for protein levels of OXPHOS genes in young and old iNs. The blot shows, from large to small: ATP5A (Complex V, cV), UQCRC2 (Complex III, cIII), SDHB (Complex II, cII), and COXII (Complex IV, cIV, mtDNA-encoded). Quantitative data was normalized to VDAC.

(**E**) Quantitative RT-PCR (qPCR) for the mtDNA-encoded gene MT-ND1 in aging iNs. Expression data were normalized to GAPDH.

(**F**) Western blot for the mtDNA-encoded gene MT-ND1 in aging iNs shows low protein levels that decrease with age.

(**G**) Relative expression of mitochondrial ribosomal proteins (MRPs) in in young and old iNs. VST normalized counts normalized to young; dots indicate mean ± SEM; significance values calculated by Wilcoxon test.

Figure S2. Neurite and neuronal morphologies of young and old iNs, and Antioxidant-, FOXO-, and HIF1a-related gene expression in aging iNs Related to Figure 2

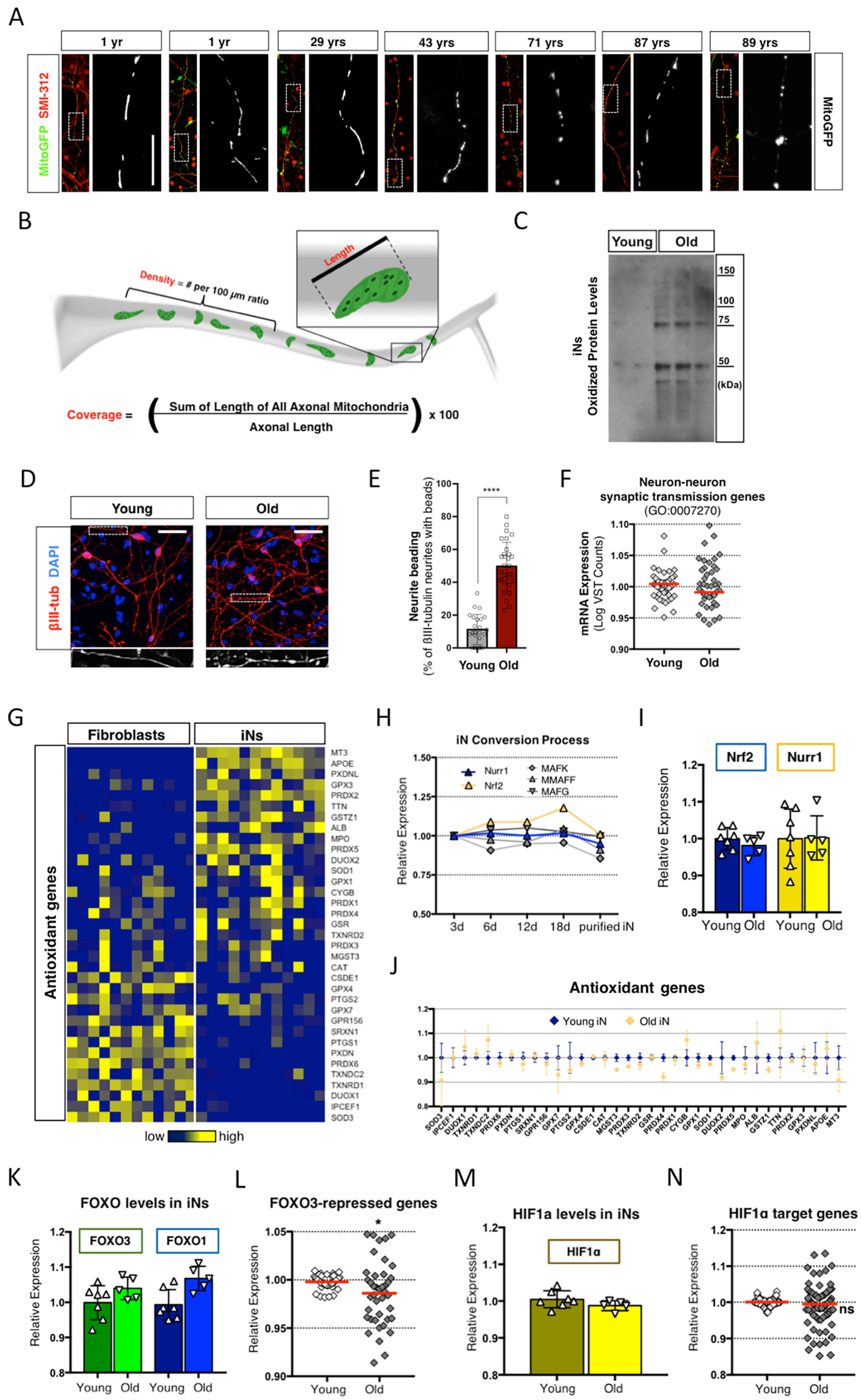

(**A**) Images of mitochondria expressing hSyn::MitoEGFP (green) with axon maker SMI-312 (red) in young and old iNs. Right panels indicate magnified images from boxed regions in the left panels. Scale bar: 20 µm

(**B**) Schematic drawing of iN axonal mitochondrial morphology indexes: length, density and coverage.

(**C**) Representative OxyBlot for oxidized proteins in young and old iNs.

(**D**) Representative immunofluorescence images of young and old iNs stained for βIII-tubulin and Dapi. Magnified examples show severe neurite beading in old, but not in young iNs.

(**E**) Quantification of neurite beading (% of βIII-tubulin neurites that show beading) in young and old iNs. Bars indicate mean ± SD; symbols represent data from individual images.

(**F**) Relative expression of Neuron-neuron synaptic transmission genes (GO:0007270) in in young and old iNs. VST normalized counts normalized to young; dots indicate mean ± SEM; significance values calculated by Wilcoxon test.

Significance values in this figure: ****$p < 0.001$.

(**G**) Heatmap showing relative expression of antioxidant genes in fibroblasts and iNs (n=12 each). Genes were sorted by FoldChange in expression from iN-enriched (top) to fibroblast-enriched (bottom) genes.

(**H**) Expression of the antioxidant regulators Nurr1 and Nrf2, an its co-factors, over the time course of iN conversion in bulk cultures, and in purified iNs at day 18.

(**I**) Relative expression of Nrf2 and Nurr1 in young and old iNs (n = 12 donors, triangles depict individuals). Bars indicate mean ± SD.

(**J**) Relative expression of antioxidant genes in young and old iNs (n = 12 donors). Symbols indicate mean ± SEM.

(**K**) Relative expression of FOXO3 and FOXO1 in young and old iNs (n = 12 donors, triangles depict individuals). Bars indicate mean ± SD.

(**L**) Expression of 41 previously validated FOXO3 target genes that become repressed as a result of FOXO3 activity (Delpuech et al. 2007; symbols mark individual genes). Significance value: *$p < 0.05$.

(**M**) Relative expression of HIF1α in young and old iNs (n = 12 donors, triangles depict individuals). Bars indicate mean ± SD.

(**N**) Relative expression of HIF1α target genes in young and old iNs (n = 12 donors). Bars indicate mean ± SD. Symbols mark individual genes. Significance value: *$p < 0.05$.

Figure S3. Rejuvenated neurons from young- and old-derived iPSCs, Related to Figure 3

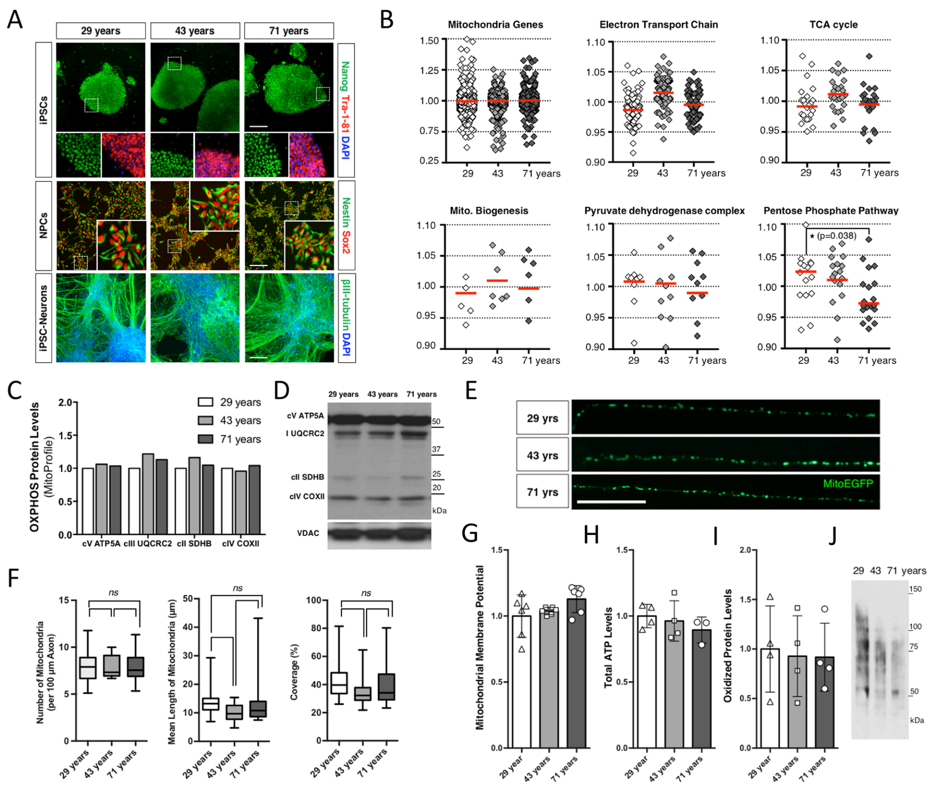

(**A**) Representative images of immunofluorescent characterization of young (29 years), mid (43 years) and old-derived (71 years) iPSCs for Nanog and Tra-1-81, iPSC-derived neural progenitor cells (NPCs) for Nestin and Sox2, and iPSC-Neurons for ßIII-tubulin. Scale bars = 100 µm.

(**B**) Expression of functional gene groups in young, mid and old-derived iPSC-Neurons. Logarithmic VST normalized counts; bars indicate mean values; dots represent genes; the non-parametric Wilcoxon test was used to determine if significance differences exist. Significance values: *$p < 0.05$.

(**C**-**D**) Relative protein levels of OXPHOS proteins in young and old iNs assessed by quantitative MitoProfile Western blot (n = 3 individuals). No significance detected by t-test.

(**E**) Representative images of MitoGFP-labeled mitochondria in neurites of young, mid and old-derived iPSC-Neurons. Scale bar = 100 µm.

(**F**) Quantification of axonal mitochondrial morphologies for densities, mean lengths and coverage in iPSC-Neurons (6 experimental replicates per individual). Box plots show 25th to 75th percentiles, bars indicate medians, and whiskers show ranges. Significance values calculated by unpaired t-tests.

(**G**) Quantification of the MMP in iPSC-Neurons (6 replicates per individual). Bar graph shows means ± SD, triangles indicate individual measurements. Significance values calculated by Mann-Whitney test.

(**H**) ATP levels in iPSC-Neurons (4 replicates per individual). Bar graph shows means ± SD, triangles indicate individual measurements. Significance values calculated by Mann-Whitney test.

(**I**-**J**) Quantification and representative image of oxidized protein levels (OxyBlot) in iPSC-Neurons.

Figure S4. Mitochondrial features in aging fibroblasts, Related to Figure 3

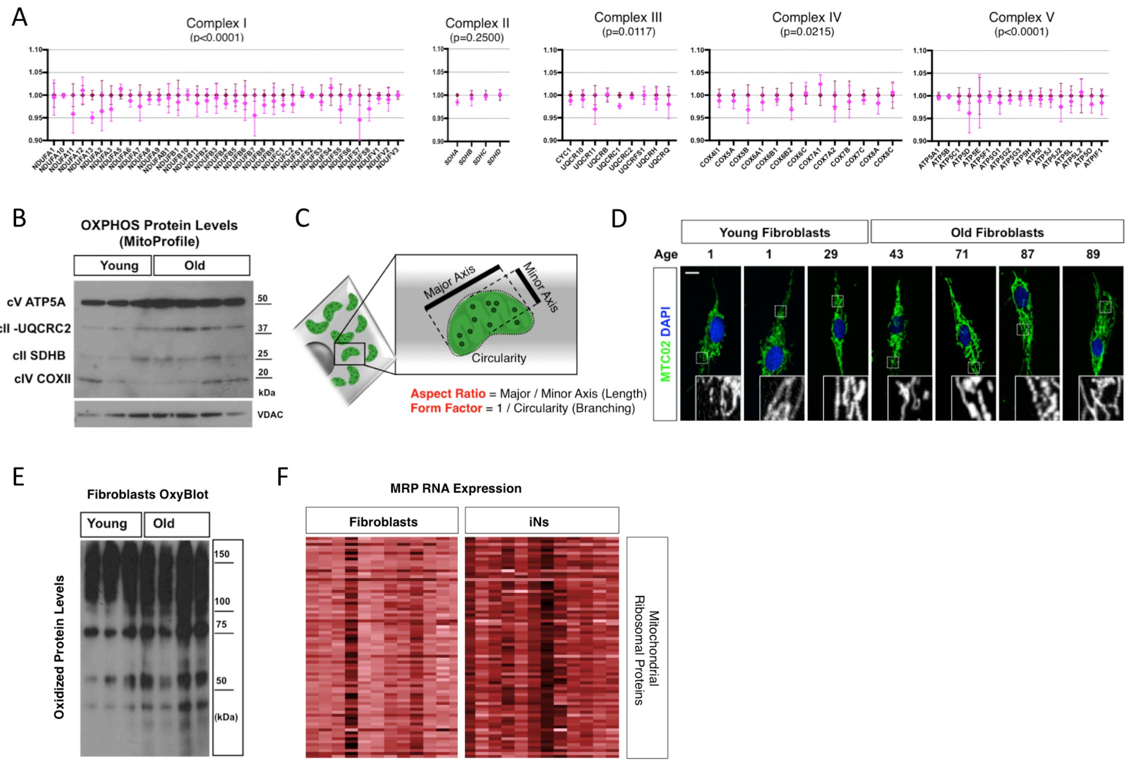

(**A**) Relative expression of ETC complex I, II, III, IV and V in young and old fibroblasts. VST normalized counts normalized to young; dots indicate mean ± SEM; significance values for each complex calculated by Wilcoxon test.

(**B**) Representative MitoProfile blot for protein levels of indicated OXPHOS genes in young and old iNs. Quantitative data was normalized to VDAC.

(**C**) Schematic diagram of fibroblast mitochondrial morphology indexes: aspect ratio and form factor.

(**D**) Images of mitochondria with mitochondrial marker (anti-MTC02 antibody, green) and DAPI (blue) in young and old fibroblasts. The bottom panels indicate magnified images of MTC02 from boxed regions. Scale bar: 20 µm.

(**E**) Representative OxyBlot for oxidized proteins in young and old fibroblasts.

(**F**) Heatmap showing relative expression of mitochondrial ribosomal protein (MRP) genes in 12 fibroblast and 12 iN cultures. Darker color indicates higher expression. See also Table S3.

Table S1. Human fibroblasts used in this study, Related to Supplemental Experimental Procedure

Age [yr]	ID	Full Name	Sex	Health	Fibroblast Source	Fibroblast RNAseq Passage
0	BJ	BJ CRL-2522	m	healthy	ATCC	p13
0	GM	GM22159	m	healthy	Coriell	p16
1	O6	AG08498	m	healthy	Coriell	p16
1	G59	GM05659	m	healthy	Coriell	p16
29	A54	AG04054	m	healthy	Coriell	p5
29	E1	ERF1	f	healthy	Erlangen	p10
30	A53	AG13153	m	healthy	Coriell	p5
43	E4	UKERf1JF-X-001	m	healthy	Erlangen	p12
66	A03	AG07803	m	healthy	Coriell	p14
71	E30	UKERfO3H-X-	m	healthy	Erlangen	p11
87	A84	AG10884	m	healthy	Coriell	p10
89	A29	AG13129	m	healthy	Coriell	p9

Table S2. Antibodies, Related to Supplemental Experimental Procedure

Antigen and species	Manufacturer	ICC dilution	WB dilution
MTC02 ms	Abcam	1:500	
SDHB ms	Abcam		1:1,000
UQCRC2 ms	Abcam		1:1,000
COXII ms	Abcam		1:1,000
ATP5A ms	Abcam		1:1,000
VDAC rb	Cell Signaling Technology		1:1,000
SMI-312 ms	Abcam	1:200	
TuJ rb	Millipore	1:3000	
vGlut rb	Synaptic Systems	1:1000	
GABA rb	Sigma Aldrich	1:300	
Map2ab chick	Sigma Aldrich	1:500	
MTC02	Thermo Fisher Scientific	1:100	
Nanog gt	R&D Systems	1:200	
Tra-1-81 ms	Millipore	1:200	
Sox2 rb	Cell Signaling	1:250	
Nestin ms	Millipore	1:200	

Conjugate and species detected	Manufacturer	ICC dilution	WB dilution
Alexa488 rb ms	Thermo Fisher Scientific Scientific	250	
Alexa647 ms-IgG chicken	Thermo Fisher Scientific Scientific	250	
Alexa555 rb ms	Thermo Fisher Scientific Scientific	250	
HRP rb ms	Jackson		5,000

Supplemental Experimental Procedures

Fibroblasts culture and direct conversion into iNs. Primary human dermal fibroblasts from donors between 0 and 89 years of age were obtained from the Coriell Institute Cell Repository, the University Hospital in Erlangen and ATCC (Table S1). Protocols were previously approved by the Salk Institute Institutional Review Board and informed consent was obtained from all subjects. Fibroblasts were cultured in DMEM containing 15% tetracycline-free fetal bovine serum and 0.1% NEAA (Thermo Fisher Scientific), transduced with lentiviral particles for EtO and XTP-Ngn2:2A:Ascl1 (N2A) and expanded in the presence of G418 (200 µg/ml; Thermo Fisher Scientific) and puromycin (1 µg/ml; Sigma Aldrich) as 'iN-ready' fibroblast cell lines. Following at least 3 passages after viral transduction, 'iN-ready' fibroblasts were trypsinized and pooled into high densities (30.000 – 50.000 cells per cm^2; appx. a 2:1 - 3:1 split from a confluent culture) and, after 24h, the medium was changed to neuron conversion (NC) medium based on DMEM:F12/Neurobasal (1:1) for 3 weeks. NC contains the following supplements: N2 supplement, B27 supplement (both 1x; Thermo Fisher Scientific), doxycycline (2 µg/ml, Sigma Aldrich), Laminin (1 µg/ml, Thermo Fisher Scientific Scientific), dibutyryl cyclic-AMP (500 µg/ml, Sigma Aldrich), human recombinant Noggin (150 ng/ml; Preprotech), LDN-193189 (5 µM; Fisher Scientific Co) and A83-1 (5 µM; Santa Cruz Biotechnology Inc.), CHIR99021 (3 µM, LC Laboratories), Forskolin (5 µM, LC Laboratories) and SB-431542 (10 µM; Cayman Chemicals). Medium was changed every third day. For further maturation up to 6 weeks, iNs were switched to BrainPhys (STEMCELL Technologies)-based neural maturation media (NM) containing N2, B27, GDNF, BDNF (both 20 ng/ml, R&D), dibutyryl cyclic-AMP (500 µg/ml, Sigma Aldrich), doxycycline (2 µg/ml, Sigma-Aldrich) and laminin (1 µg/ml, Thermo Fisher Scientific Scientific). For maturation on astrocytes for morphological analysis, iNs were carefully trysinized during week 4 and replated on a feeder layer of mouse astrocytes and cultured in NM media containing 1% KOSR (Thermo Fisher Scientific).

Mitochondrial morphological analysis in iNs and fibroblasts. Following conversion for 3 weeks, iNs were transduced with a lentiviral vector encoding MitoEGFP under the human synapsin promoter (hSyn) and subsequently cultured on a layer of mouse astrocytes for another 3 weeks (6 weeks in total). The fibroblasts were plated on a µ-slide 8-well slides (Ibidi, Germany). The cells were fixed in 4% paraformaldehyde and 4% sucrose and then permeabilized with 0.05% Triton-X100 in Tris-Cl buffer solution (TBS). The cells were then blocked in TBS containing 3% bovine serum albumin (BSA) for 1 h, followed by incubation with primary antibody overnight at 4°C. After 4 time washes with TBS, cells were incubated with secondary antibodies for 1 h at room temperature. Following 3 time washes with TBS, cells were incubated with DAPI (0.1 µg/ml, Sigma) for 15 min, followed by 3 time washes with TBS to remove DAPI. Fluorescent signals were detected using a LSM780 confocal microscopy (Carl Zeiss). The primary antibodies used were mouse anti-MTC02 antibody (1:500, abcam, ab3298) and mouse anti-pan axonal neurofilament antibody (1:200, Abcam, SMI-312, ab24574). The GFP signal (MitoEGFP) and green fluorescence (MTC02) were used to analyze the mitochondrial number, size, coverage, aspect ratio, and form factor using the Particle Analysis tool in ImageJ software (National Institute of Health).

Whole transcriptome mRNA sequencing and analysis. Following 3 weeks of iN conversion, iNs were detached and stained for PSA-NCAM (1:100; PE- or APC-coupled from BD Biosciences) for 45 min at 4°C, resuspended in sorting buffer containing EDTA and DNAse and filtered using a 40-µm cell strainer. The PSA-NCAM-positive population was sorted directly into Trizol-LS and RNA was isolated according to the manufacturer's instructions and digested with TURBO DNAse (Thermo Fisher Scientific). RNA from fibroblasts was directly extracted from confluent cultures. RNA integrity (RIN) numbers were assessed using the Agilent TapeStation before library preparation. RNA-Seq libraries were prepared using the TruSeq Stranded mRNA Sample Prep Kit according to the manufacturer's instructions (Illumina). Libraries were sequenced single-end 50 bp using the Illumina HiSeq 2500 platform. Read trimming was performed using TrimGalore, read mapping was performed using STAR, raw counts were generated using HTseq and variance stabilizing transformation normalization (vst) and differential expression analysis was performed in DEseq2. Filtering for 1,158 mitochondrial genes was performed using the Human MitoCarta 2.0 atlas from the Broad Institute (Table S3).

Western blotting. Cell lysates were prepared in Lysis buffer A (20mM Tris pH 7.5, 100mM NaCl, 1mM EDTA, 2mM EGTA, 50 mM β -glycerophosphate, 50 mM NaF, 1 mM sodium vanadate, 2 mM dithiothreitol, proteinase inhibitor cocktail (Roche) and 1% Triton X-100) and subjected to Western blot according to the standard procedures. The primary antibodies used were mouse anti-Total OXPHOS human WB antibody (1:1000, Abcam, ab110411) and rabbit monoclonal anti-VDAC antibody (1:1000, Cell Signaling, D73D12, #4661). All relevant information of the antibodies used in this study including citation, clone number and antibody validation profile can be found at the manufacturer's website (Table S2). OxyBlot (Abcam) detection of oxidized proteins was used as recommended in the manufacturer's manual.

ATP analysis. For measurement of cellular ATP content, the cells were lysed directly on plates with passive lysis buffer (Promega) by 2 freeze-and-thaw cycles (-20°C). The ATP content was quantified by Cell Titer-Glo Luminescent Cell Viability/ATP Assay kit (Promega) using Victor X Lite Multilabel Plate Reader (PerkinElmer) and normalized by protein content measured by a Pierce BCA protein assay kit (Thermo Fisher Scientific Scientific).

Immunocytochemistry. Cells were washed with PBS and fixed with 4% paraformaldehyde (PFA, 20 min, RT) and blocked with 5% horse serum in PBS and 0.1% TritonX-100. Primary antibodies (Table S2) were incubated overnight at 4°C, washed for 5 min with DAPI solution, incubated with secondary antibodies (Table S2) for 45 min at room temperature (RT) and mounted in PVA-DABCO (Sigma Aldrich) or Shandon Immu-Mount mounting solution (fisher scientific). For confocal imaging, cells were grown on ibidi μ-slides. Antibodies are listed in Supplemental Table S2.

Quantitative RT PCR. RNA was isolated using Trizol and subsequently reversely transcribed using SuperScript III Reverse Transcriptase (Thermo Fisher Scientific). qPCR was performed using SYBRgreen Real-Time Mastermix (BioRad) and fold changes of mRNA levels were calculated using the delta-delta-Ct method using Microsoft Excel. The following primer sequences were used: GAPDH (fw: TGACAACTTTGGTATCGTGGA, rv: CCAGTAGAGGCAGGGATGAT), MT-ND1 (fw: ATGGCCAACCTCCTACTCCT, rv: GCGGTGATGTAGAGGGTGAT),

iPSC reprogramming and neuronal differentiation.
Fibroblasts were transduced with retroviruses for the four Yamanaka factors and resulting iPSC lines were cultured in STEM-TeSR (Salk Stem Cell Core) on BME matrix-coated (Trevigen) dishes. Following neural differentiation into neural progenitor cells (previously described in Boyer L et al., Current Protocols in Stem Cell Biology 2012), neuronal differentiation was induced by growth factor withdrawal. For RNAseq, PSA-NCAM-positive (Miltenyi) and CD29-low (BD) neurons were isolated by FACS.

Statistical analysis. Statistical values for RNA-Seq data were corrected for false discovery rates (FDR) using the Benjamini-Hochberg method implemented in R. Statistical tests of quantitative data were calculated using GraphPad Prism 7 software with the method indicated for each figure. Significance evaluation are marked as *$p<0.05$; **$p<0.01$; ***$p<0.005$ and ****$p<0.001$.